Physical Chemistry Chemical Physics Accepted Manuscript

Kinetics of the ClO + CH$_3$O$_2$ reaction over the temperature range T = 250 – 298 K

Michael K.M. Ward[†] and David M. Rowley*

*Department of Chemistry, UCL, 20 Gordon Street, London WC1H 0AJ, UK.
[†]-Laboratoire PC2A/CNRS, Université de Lille 1, 59655, Villeneuve d'Ascq, France

Abstract

The kinetics of the potentially atmospherically important ClO + CH$_3$O$_2$ reaction (1) have been studied over the range T = 250 – 298 K at p = 760 Torr using laser flash photolysis radical generation, coupled with time resolved ultraviolet absorption spectroscopy, employing broad spectral monitoring using a charge coupled device detector array. ClO radicals were monitored unequivocally using this technique, and introduction of CH$_3$O$_2$ precursors ensured known initial methylperoxy radical concentrations. ClO temporal profiles were thereafter analysed to extract kinetic parameters for reaction (1). A detailed sensitivity analysis was also performed to examine any potential systematic variability in k_1 as a function of kinetic or physical uncertainties. The kinetic data recorded in this work show good agreement with the most recent previous study of this reaction, reported by Leather *et al.*[14] The current work reports an Arrhenius parameterisation for k_1, given by:

$$k_{(1)}(T) = 2.2^{+3.4}_{-1.3} \times 10^{-11} \, e^{\left(\frac{-(642 \pm 253)\,\mathrm{K}}{T}\right)} \mathrm{cm^3 \; molecule^{-1} \; s^{-1}}$$
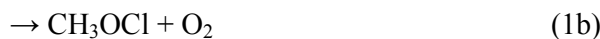
This work therefore concurs with that of Leather *et al.*[14] implying that the title reaction is potentially less significant in the atmosphere than inferred from preceding studies. However, reaction (1) is evidently a non-terminating radical reaction, whose effects upon atmospheric composition therefore need to be ascertained through atmospheric model studies.

1. Introduction

It is well established that atmospheric halogen atoms, released from photolysis of anthropogenic or natural borne halogenated pollutants, or from heterogeneous processes, initiate oxidative loss of many trace species in the air.[1] Most notably, halogen atoms react with ozone in both the troposphere and the stratosphere, leading to the formation of halogen oxide free radicals, XO, (X = Cl, Br, I). Subsequent reactions of XO which thereafter regenerate halogen atoms lead to catalytic processes which augment the effect of halogens on atmospheric composition. Most notably, ClO radicals are implicated in stratospheric ozone loss, particularly in Polar regions in Springtime, but also at midlatitudes.[2,3] Additionally XO radicals deplete ozone in the troposphere, where their effect is to alter the oxidative capacity of the air, leading to potential changes in the budget of pollutants, including those of greenhouse gases.[4] Halogen atoms may also react with organic species in the air, typically for saturated organic species resulting in hydrogen abstraction and the generation of alkyl radicals and, in the presence of excess oxygen, the formation of alkylperoxy, RO_2, species. Principally, RO_2 radicals emerge from the oxidation of organic pollutants by OH radicals, which are generated following the photolysis of ozone. Whilst XO radicals have a generally deleterious effect on atmospheric ozone (and other trace species), the reactions of RO_2 may affect ozone abundances through the removal of oxidising radicals (OH, HO_2, RO_2) or, in the presence of other pollutants, notably nitrogen oxide species, NO and NO_2, to the production of oxidising species such as ozone, with potential implications for oxidative capacity, air quality and photochemical smog formation.

Whilst individual halogen oxide and peroxy radical family chemistries have a proven and well-quantified effect on atmospheric composition, the coupling between such radical families is also important. The ClO + HO_2 reaction, for example has been implicated in midlatitude stratospheric ozone loss.[5] The ClO + CH_3O_2 (1) reaction is similarly important, as first recognised by Crutzen *et al.*[6] The current work details studies of the kinetics of the ClO + CH_3O_2 reaction (1), on account of its potential atmospheric importance.

There have been a number of previous studies of reaction (1), investigating the kinetics and/or product distribution as a function of temperature.[7,8,9,10,11,12,13,14] Unlike the analogous reaction of ClO with HO_2, there is, in this case, a possible radical non-terminating channel (1a):

$$ClO + CH_3O_2 \quad\quad \rightarrow ClOO + CH_3O \quad\quad\quad (1a)$$
$$\rightarrow CH_3OCl + O_2 \quad\quad\quad (1b)$$
$$\rightarrow HCHO + HCl + O_2 \quad\quad\quad (1c)$$

The products of channel (1a) lead to the formation of Cl *via* the subsequent thermal decomposition of ClOO and the reaction of CH_3O with oxygen results in the formation of HO_2. Both of these radical products thereafter re-enter catalytic cycles, thus the branching of reaction (1) has atmospheric implications concerning both the stratospheric ozone and odd hydrogen (HO_x) budgets.[15]

The kinetics and product branching of the $ClO + CH_3O_2$ reaction were first studied at ambient temperature by Simon *et al.*[7] employing the broadband photolysis of $Cl_2/Cl_2O/CH_4/O_2$ mixtures, using molecular modulation UV absorption spectroscopy detection at $p = 310$ mbar. Helleis *et al.*[8,9] thereafter investigated the absolute rate coefficient and the branching ratio, $k_{(1a)}/k_1$ as a function of temperature ($T = 215 – 295$ K) and pressure ($p = 2.3 – 4.0$ mbar) using a flow tube technique with mass spectrometric (MS) detection. A study from Kenner *et al.*[10] in the same year measured the absolute rate coefficient of reaction (1) at $T = 293$ K and $p = 2.5$ mbar again using the flow tube/ MS technique. Kukui *et al.*[11] measured k_{1a}/k_1 and the absolute rate coefficient k_1 from $T = 233 – 300$ K in a flow tube at $p = 5 – 6$ mbar, monitoring both parent ions *via* mass spectrometry. A further two flow tube investigations of the branching k_{1a}/k_1 at room temperature ($T = 298$ K) were reported by Biggs *et al.*[12] and Daele and Poulet[13] at $p = 2.7$ mbar and $p = 1.3$ mbar respectively. These studies used mass spectrometry and laser induced fluorescence to detect ClO and CH_3O respectively. The most recent study of reaction (1) was that of Leather *et al.*[14] who measured the absolute rate coefficient k_1 as a function of pressure ($p = 100 – 200$ Torr) and temperature ($T = 298 – 223$ K) using a turbulent flow technique with a chemical ionisation mass spectrometry detection system.

There is general agreement from the above studies that channels (1a) and (1b) are the only significant pathways operating at stratospheric temperatures. However, there is considerable disagreement concerning the relative importance of these two channels with a number of studies reporting conflicting findings concerning as to which one is dominant. As a consequence of this discrepancy, NASA-JPL[16] do not recommend a branching ratio for

reaction (1). This branching ratio has, however, direct implications for the extraction of the overall rate constant for reaction (1) from kinetic measurements, as discussed below.

Helleis *et al.*,[8,9] Kukui *et al.*,[11] Kenner *et al.*,[10] Simon *et al.*[7] and Leather *et al.*[14] report ambient temperature determinations of k_1. The temperature dependence of this reaction has also been reported by Helleis *et al.*,[8,9] Kukui *et al.*[11] and Leather *et al.*[14] These kinetic parameters are shown in Table 1. It is interesting to note that Helleis *et al.*[8,9] and Kukui *et al.*[11] report only a slight temperature dependence to reaction (1) albeit with opposite temperature dependences. By contrast the more recent study of Leather *et al.*[14] reports a much stronger positive temperature dependence, with a *E/R* value over 5 times that reported by Helleis *et al.*[8,9]

Simon *et al.*,[7] Helleis *et al.*[8,9] and Kukui *et al.*[11] all report channel (1a) being the dominant pathway at $T = 298K$ whereas later studies from Biggs *et al.*[12] and Daele and Poulet[13] report (1a) as being the minor channel. This discrepancy may also affect evaluation of the overall rate constant, discussed below.

Computational studies shed further light on the mechanism of reaction (1) and corroborate some experimental studies on the possible product channels. A computational characterization of reaction (1) was reported by Kosmas *et al.*[17] The calculations suggest a viability of the two important channels observed experimentally, leading to $CH_3O + ClOO$ (1a) and $CH_3OCl + O_2$ (1b) products. Specifically, a re-evaluation of the exothermicity of channel (1a) using spin-restricted methods, suggests this channel as the most important pathway. The methyl hypochlorite production, channel (1b), is also shown to be thermodynamically feasible through either the singlet or the triplet surface. Finally, a fourth channel:

$$ClO + CH_3O_2 \quad \rightarrow \quad CH_2O + HOOCl \quad\quad (1d)$$
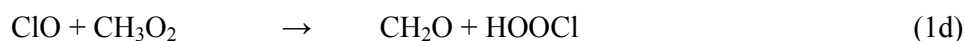
was also found to be thermodynamically accessible, with the HOOCl product predicted to dissociate readily into HCl and O_2.

Thus, whilst the kinetics of the $ClO + CH_3O_2$ reaction appear well-established at ambient temperature, the considerable uncertainties in the temperature dependence of this reaction preclude agreement between studies at lower atmospheric temperatures. The uncertainties in the branching ratio for reaction (1) also directly affect the evaluation of k_1. The current work

has determined k_1 using a well constrained chemical system, using broadband spectral monitoring of ClO radicals. Detailed sensitivity analyses have been carried out and quantified the potential uncertainty arising from assumptions made in previous work. The kinetics of reaction (1) are reported and the potential atmospheric implications of these are briefly discussed.

2. Experimental

2 (i) Principles of the experiment

The ClO + CH_3O_2 reaction was studied using laser flash photolysis of suitable precursor gas mixtures coupled with time-resolved broadband UV absorption spectroscopy. ClO radicals were monitored unequivocally using this detection, and the introduction of CH_3O_2 precursors thereafter led to a perturbation of the initial (immediate post photolysis) ClO concentration, and an enhanced decay rate of ClO, which was analysed using numerical integration and fitting, to determine the kinetics of the ClO + CH_3O_2 reaction. A sensitivity analysis was carried out to quantify the effect of model uncertainties on the derived kinetic parameters and reaction branching.

2 (ii) Radical generation

Radicals were generated following laser flash photolysis of precursor mixtures, prepared in a continuous flow of a carrier gas, typically oxygen or synthetic air. Precursor concentrations and consequently requisite gas flow rates, were initially designed using numerical integration simulations of all known radical formation chemistry given below. These concentrations were designed such that the formation of radicals immediately post-photolysis was stoichiometric and rapid on the timescale of their subsequent decay.

ClO radicals were generated following $\lambda = 351$ nm excimer laser photolysis of Cl_2/ Cl_2O/ O_2 mixtures. The principal source of ClO radicals resulted from the reaction of photolytically generated Cl atoms with an excess of dichlorine monoxide, Cl_2O.

$$Cl_2 + h\nu \quad \rightarrow \quad 2\ Cl \tag{2}$$

$$Cl + Cl_2O \quad \rightarrow \quad Cl_2 + ClO \tag{3}$$

The direct photolysis of Cl_2O also presented a minor source of ClO radicals and Cl atoms.

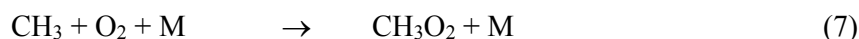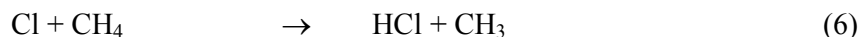$$Cl_2O + h\nu \quad \rightarrow \quad Cl + ClO \tag{4}$$
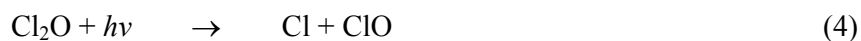
Cl$_2$O was generated *in situ* using the method originally described by Hinshelwood and Pritchard,[18] wherein a known flow of (diluted) chlorine gas passed through a trap containing dried mercury(II) oxide powder.

$$2Cl_2(g) + HgO(s) \quad\rightarrow\quad Cl_2O(g) + HgCl_2(s) \tag{5}$$
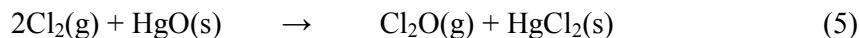
Typically, the conversion (loss) of Cl$_2$ to Cl$_2$O was above 80 %, as verified by spectroscopic measurements in this and previous work,[19] However, a T-junction in the chlorine gas line was also placed upstream of the HgO trap to partially bypass this trap and a needle valve allowed the control of the amount of Cl$_2$ which passed through the trap in order to vary (lower) this conversion thereby to optimise the initial ClO concentration.

The direct photolysis of Cl$_2$O contributed the minor source of ClO, due to the smaller cross-section of Cl$_2$O compared to Cl$_2$ at the 351nm photolysis laser wavelength (σ_{Cl_2} (351nm) = 1.8 $\times$ 10^{-19} cm^2 molecule^{-1}, σ_{Cl_2O} (351nm) = 7.0 $\times$ 10^{-21} cm^2 molecule^{-1}).[16] Precursor concentrations were: [Cl$_2$] = (2.5 − 3.5) × 10^{16} molecule cm^{-3}; [Cl$_2$O] = (1.0 − 2.0) × 10^{15} molecule cm^{-3}. Typical initial total (post photolysis) radical concentrations were in the range (0.7 − 1.5) × 10^{14} molecule cm^{-3}.

CH$_3$O$_2$ radicals were generated by reaction of photolytically generated chlorine atoms with methane, [CH$_4$] = (0.2 − 1.5) × 10^{19} molecule cm^{-3} in the presence of an excess of oxygen.

$$Cl_2 + h\nu \quad\rightarrow\quad 2\,Cl \tag{2}$$
$$Cl + CH_4 \quad\rightarrow\quad HCl + CH_3 \tag{6}$$
$$CH_3 + O_2 + M \quad\rightarrow\quad CH_3O_2 + M \tag{7}$$

The apparatus for this radical generation and monitoring has been described in detail previously and its adoption here was identical to that employed in our recent studies of the ClO + HO$_2$ and ClO + BrO reactions.[5,20,21] Briefly, gas mixtures were prepared in a continuous flow of oxygen or synthetic air in a mixing line using calibrated mass flow controllers or PTFE needle valves. These gases (used as supplied, > 99.9 % purity) were flowed into a temperature controlled reaction cell and excimer laser photolysis was achieved

by coupling laser output through cylindrical expansion lenses and dichroic reflectors longitudinally through the 1 metre long reaction cell. Output from a 75W xenon lamp counterpropagated the photolysis laser beam. This transmitted light was focussed onto a 0.25 m focal length Czerny-Turner (toroidal) spectrograph (diffraction grating 600 g/mm and slit width 112 nm, to achieve a spectral resolution of 0.8 nm full width half maximum, as verified by recording output from a mercury 'pen-ray' lamp) and then on to a charge coupled device (CCD) detector array. The top rows of the 2 dimensional array were illuminated by the transmitted light, and charge transfer routines were used to shift signal, row by row, from the illuminated region into a storage region of the device. In this way, typically 800 sequential transmission spectra through the pre- and post- photolysed gas were continuously recorded, typically for this work on a timescale of 100 μs/ spectrum. For each experiment, 50 photolysis experiments were carried out and the results co-added. At least six determinations were conducted at each experimental temperature, covering the concentration ranges indicated above.

2 (iii) Radical Monitoring

As discussed above, ClO radicals were monitored using UV absorption, in this case over the wavelength range $\lambda = 265 - 296$ nm, covering the $(A^2\Pi \leftarrow X^2\Pi)$ vibronic transition of ClO.

Data were recorded continuously before, during and after laser photolysis. Recorded transmissions were converted into wavelength and time resolved absorbances, $A_{\lambda,t}$, relative to the pre-photolysis transmitted intensities using Beer's Law:

$$A_{\lambda,t} = \frac{\langle I_{\lambda,0} \rangle}{I_{\lambda,t}} \tag{i}$$

Where $\langle I_{\lambda,0} \rangle$ is the *average* pre-photolysis transmitted light intensity at wavelength λ and $I_{\lambda,t}$ is the transmitted light intensity at wavelength λ and any time *t*. The recorded absorbances therefore exhibited *changes* in absorption brought about by laser photolysis and subsequent gas phase chemistry.

2. (iv) Determination of ClO concentrations

The concentration of ultraviolet absorbing species in the reaction vessel is related to absorbance by the Beer-Lambert law:

$$A_{\lambda,t} = \sum_i \sigma_{\lambda,t}.[i]_t.l \qquad\qquad (ii)$$

Where $A_{\lambda,t}$ is the absorbance at a wavelength λ and time t, $\sigma_{\lambda,t}$ is the absorption cross-section of absorbing species i at wavelength λ and l is the optical path length through the reaction mixture. These products are summed over the number of absorbers, i, present.

In the present work, over the wavelength range covered, multiple UV absorbing species, including precursor gases, radicals and reaction products were present, spectra for which are shown in Figure 1. For many of these species, the UV absorption spectra are evidently spectrally structureless, and whilst in principle their contributions to the total absorption could be deconvoluted, in practice the similarities and overlap of the spectra precluded this, even using broadband spectral monitoring. By contrast, ClO radicals exhibit a distinctive spectral structure as a result of the ($A^2\Pi \leftarrow X^2\Pi$) vibronic transition. This structure was exploited to determine ClO concentrations using 'differential' spectroscopy. In this procedure, the recorded absorption spectrum exhibiting the ClO spectral structure is high-pass filtered. A suitable reference spectrum of ClO is then analogously filtered and the filtered spectrum fitted to the experimental spectrum, minimising the sum of squares of residuals to determine the ClO species concentration using the Beer Lambert law (ii), and also as described in detail previously.[22],[23] In this way, the ClO concentration as a function of time was unequivocally extracted from the time resolved spectra recorded on the CCD, despite the presence of many other absorbing species in the spectral window studied.

Critical to the spectral fitting and the accuracy of [ClO] determination is that the instrumental resolution adopted is that at which the ClO absorption cross-sections are used, since the ClO vibronic cross-sections are a strong function of instrumental resolution. In this work, a spectral resolution of 0.8 nm FWHM was chosen. This resolution is identical to that employed by Ferracci and Rowley[22] and Boakes *et al.*[24] from which the extensively studied ClO absorption cross-sections, and from which their temperature dependence, were taken.

The temperature dependent 'differential' absorption cross-sections for the representative 12-0 vibronic band of ClO, corresponding to the difference between the peak at $\lambda = 275.2$ nm minus the trough at $\lambda = 276.4$ nm were given by:

$$\sigma_{ClO\ diff}/\text{cm}^2\ \text{molecule}^{-1} = (1.07 \pm 0.33) \times 10^{-17} - \left\{ (2.46 \pm 1.1) \times 10^{-20}.(T/\text{K}) \right\} \qquad \text{(iii)}$$

Whilst these two wavelengths were used at which to calibrate the ClO differential absorbance, it should be noted that a time-resolved spectrum recorded over the *entire* range $\lambda = 265 - 296$ nm was recorded at each time point, and the spectral fitting adopted all of this range in determining $[\text{ClO}]_t$.

3. Kinetic analysis and results

Figure 2 shows time averaged post-photolysis (relative to pre-photolysis) absorption spectra, recorded in the absence and presence of methane ($[CH_4] = 5.25 \times 10^{18}$ molecule cm^{-3}), under otherwise identical circumstances. The vibronic spectral structure of ClO is evident, as is the reduction in the ClO absorbance upon the introduction of methane.

Temporal traces of [ClO] were obtained from sequential spectra obtained as described above. Such traces were initially recorded in the absence of methane, showing reversible ClO dimerization, then in the presence of methane over the range of concentrations given above, and thereafter with methane removed from the system. Example traces are presented in Figure 3. Evidently, ClO dimerises reversibly to equilibrium. Then the addition of methane reduces the initial post photolysis ClO concentration, but also leads to an enhancement in the rate of ClO loss. This reverts exactly to the initial behaviour in experiments following removal of methane. The initial post photolysis (maximum) [ClO] as a function of added methane is shown in Figure 4.

Given that the only effective reactive partners for methane in this photolytic system are chlorine atoms, and that the sole fate of methyl radicals thereafter formed and lost, through reactions (6) and (7), in the presence of excess oxygen, is to produce methylperoxy radicals, this indicates that, upon introduction of methane, methylperoxy radicals are produced at the expense of ClO and thereafter the ClO + CH$_3$O$_2$ reaction takes place.

3. (i) ClO in the absence of methane

The reversible ClO dimerization kinetics were analysed using a simple 2 reaction kinetic model comprising:

$$ClO + ClO + M \quad \rightleftharpoons \quad Cl_2O_2 + M \qquad (8, -8)$$
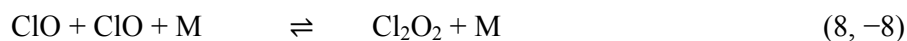
Results from this analysis are presented in Table 2 and show reasonable agreement with equivalent values calculated from the current NASA-JPL data evaluations[16] and excellent agreement with the findings of Ferraci *et al.*[22] Furthermore, the analysis of equilibrium

constants obtained from these kinetic parameters, shown in van't Hoff form in Figure 5 in comparison with the study of Ferracci *et al.* also show excellent agreement, with thermodynamic parameters $\Delta_r H° = (-86.9 \pm 5.0)$ kJ mol^{-1} and $\Delta_r S° = (-185.4 \pm 17.5)$ J K^{-1} mol^{-1} respectively (this work), compared to Ferracci *et al.*[22] $\Delta_r H° = (-80.7 \pm 2.2)$ kJ mol^{-1} and $\Delta_r S° = (-168.1 \pm 7.8)$ J K^{-1} mol^{-1}, both obtained from second law analyses. Thus, the ClO behaviour in the absence of methane is well-established and consistent with previous work and is entirely self-consistent before and after the introduction of methane. The k_8 and k_{-8} values recorded in the present work were used in the subsequent analysis of the cross-reaction.

3(ii) ClO in the presence of CH$_3$O$_2$

The observations detailed above and shown in Figures (2) and (3) show that ClO radicals are formed *via* reactions (3) and (4), but upon addition of methane to this system (in excess oxygen), CH$_3$O$_2$ radicals are produced competitively. The initial branching for nascent Cl atoms formed on photolysis can therefore be defined by a ratio θ, where:

$$\theta = \frac{k_{(6)}[CH_4]}{k_{(6)}[CH_4] + k_{(3)}[Cl_2O]} \tag{iv}$$

Given a total initial radical concentration defined from the methane-free experiments, the factor theta could thereafter be used to constrain $[ClO]_0$ and $[CH_3O_2]_0$ in the presence of methane. The behaviour of $[ClO]_0$ as a function of added methane was consistent with a Cl + Cl$_2$O *vs* Cl + CH$_4$ competition.

Thereafter the ClO decay kinetics in the presence of methane could in principle be defined through reactions (8), (−8) and (1). It is also clear that reaction (1) does occur, since a simulated temporal trace of ClO excluding the cross reaction of ClO with CH$_3$O$_2$ but with parameters taken from the methane-free experiments shows, in Figure 6, a significant deviation of the simulated ClO dimerization only profile from the observed temporal ClO trace. A simple kinetic model based upon reversible ClO dimerization including a terminating reaction of ClO with CH$_3$O$_2$ (1) could, however, fit the observed ClO temporal behaviour well, but returned enhanced apparent rate constants for reaction (1) as a function of increasing [CH$_4$]. This is unsurprising, since the well-known CH$_3$O$_2$ self reaction must operate at high

[CH$_3$O$_2$]$_0$/[ClO]$_0$ ratios and this reaction is non-terminating.[16] Specifically, the generation of CH$_3$O radicals in reaction (9a) would lead to the production of HO$_2$ radicals in reaction (10) and the subsequent additional reaction of ClO with HO$_2$. Further, as discussed above, the ClO + CH$_3$O$_2$ reaction has also itself been reported as non-terminating. Thus secondary products of channel (1a) would be expected to interact with primary radicals and enhance the observed ClO decay:

$$CH_3O_2 + CH_3O_2 \rightarrow CH_3O + CH_3O + O_2 \quad (9a)$$
$$CH_3O_2 + CH_3O_2 \rightarrow CH_3OH + HCHO + O_2 \quad (9b)$$
$$CH_3O + O_2 \rightarrow HCHO + HO_2 \quad (10)$$

On account of the significant secondary chemistry shown in this system, which is shown diagrammatically in Figure 7, a detailed kinetic model was constructed in the numerical integration package FACSIMILE, for fitting to ClO temporal profiles. This comprehensive reaction scheme is given in Table 3. The optimised parameters in the model were the initial (post photolysis) ClO concentration and the rate constants for the two dominant pathways of reaction (1). The branching for these pathways was taken from the current IUPAC recommendation. Figure 8 shows a typical model fit to an experimental [ClO]$_t$ trace. Individual traces were fit separately, owing to different sensitivity factors as a function of methane. Notably, the adoption of the full kinetic model showed no variability of the extracted rate constant k_1 with methane concentrations, as was observed with the simple three reaction model that ignored channel branching in reaction (1). The values obtained for k_1 from this analysis are plotted in Arrhenius form in figure 9, along with the corresponding Arrhenius parameterisation and the averaged values for each temperature are presented in Table 2. The parameterisation from figure 9 was described by:

$$k_{(1)}(T) = 2.2^{+3.4}_{-1.3} \times 10^{-11} \, e^{\left(\frac{-(642 \pm 253)\text{K}}{T}\right)} \text{cm}^3 \text{ molecule}^{-1} \text{ s}^{-1}$$

Where errors are 1σ, statistical only from a weighted fit to data. The corresponding NASA-JPL and IUPAC recommendations for k_1, also shown in Figure 1, are given by:

$$k_{(1)}(T) = 3.3 \times 10^{-12}\, e^{\left(\frac{-115\,\text{K}}{T}\right)} \text{cm}^3\ \text{molecule}^{-1}\ \text{s}^{-1}\ \text{(JPL NASA)}$$

$$k_{(1)}(T) = (2.40 \pm 0.15) \times 10^{-11}\, e^{\left(\frac{-(20\,\pm 200)\,\text{K}}{T}\right)} \text{cm}^3\ \text{molecule}^{-1}\ \text{s}^{-1}\ \text{(IUPAC)}$$

These recommendations are based on the studies of Helleis et al.[8] and Kukui et al,[11] with the more recent study of Leather et al.[14] yet to be incorporated. It is interesting to note that the present study has recorded a much stronger positive temperature dependence for k_1 than the current recommendations, but in good agreement with the work of Leather et al.[14] Figure 10 shows a summary of the temperature dependence studies of k_1.

3 (iii) Sensitivity analysis

The chemical system employed in this work was inherently complex, both in terms of the initial radical precursor concentrations and in terms of the subsequent radical chemistry as presented in Table 3. Further, uncertainties in parameters such as absorption cross sections could present systematic errors. Consequently, a detailed sensitivity analysis was carried out for the kinetic analysis to ascertain the potential systematic errors on the data reported here. A simulated ClO temporal trace was thus generated, using parameters as reported in Table 1, and this trace was reanalysed using a model with, in turn, each parameter perturbed by being halved or doubled. The percentage difference between k_1 returned from the perturbed model and the original was then examined. For the vast majority of reactions included in Table 3, the sensitivity was minimal, within 1 %, at all temperatures. However, the returned values of k_1 were significantly perturbed by changes in certain model parameters. Specifically, the self-reaction chemistry of ClO gave up to a 50 % perturbation in the extracted rate constant k_1, when varied by a factor of two at T = 298 K. Sensitivity to uncertainty in k_{-8} at low temperatures was however much diminished, since this reaction becomes insignificant at low temperatures. However, even this notional uncertainty of ± 50 % in the ClO dimerization equilibrium led to similarly large systematic uncertainties in k_1. Indeed, the model could not converge on a visually adequate fit to the ClO temporal profile with k_8 doubled. It should however be noted that a ± 50 % perturbation of the ClO dimerization kinetics is somewhat larger than the reported uncertainties in these kinetics and indeed at the upper limit of uncertainties recommended by NASA-JPL and IUPAC. Further, the nature of the experiments in the current work were perturbation studies: the ClO dimerization kinetics were well

established before and after the introduction of methane, under otherwise identical conditions. It is thus reasonable to assume that the dimerization kinetics were well constrained in the intervening experiments incorporating methane, hence CH_3O_2.

The sensitivity of the kinetic determinations for reaction (1) was also examined regarding systematic errors in the ClO (differential) cross section. The systematic error in the differential cross section of *ca.* $\pm$ 16 % at T = 298 K reported by Boakes *et al.*[24] results in a scaling of the [ClO] temporal trace by the same extent. The effect of the extracted rate constants for ClO dimerisation and thereby in turn reaction (1) were also examined. These were found to be typically < 15%.

Finally, importantly for a mixed radical cross-reaction in which both radicals self-react, a flux analysis was carried out. Intuitively at high $[ClO]_0/[CH_3O_2]_0$ ratios (governed by the $[Cl_2O]/[CH_4]$ ratio), the ClO self reaction dominates. Conversely, at low ratios, the methylperoxy self reaction dominates, and the greatest flux (and therefore greatest sensitivity) to the ClO + CH_3O_2 reaction lies in between. The CH_3O_2 self-reaction is the most problematic in this sense, as it is non-terminating, leading to CH_3O and thereafter HO_2 formation. The initial radical precursor ratios were therefore designed to account for this, such that methane concentrations were kept high enough to maximise the flux through reaction (1), whilst minimising the CH_3O_2 self reaction and therefore secondary (notably HO_2) chemistry which was accounted for in the above sensitivity analysis. Adopting these conditions therefore minimised the sensitivity of k_1 to the uncertainties in the ClO + HO_2 kinetics.

4. Discussion

4 (i) Comparison with previous work

At $T = 298$ K, the results from this work agree well with those of Kukui *et al.*[11] and Leather *et al.*[14] as shown in Table 1. These authors report values of k_1 ($T = 298$ K) = $(2.5 \pm 0.3) \times 10^{-12}$ cm^3 molecule^{-1} s^{-1} and k_1 ($T = 298$ K) = $(2.4 \pm 0.3) \times 10^{-12}$ cm^3 molecule^{-1} s^{-1} respectively, compared to k_1 ($T = 298$ K) = $(2.7 \pm 0.5) \times 10^{-12}$ cm^3 molecule^{-1} s^{-1} in the present work. When considering the uncertainty, the present work also agrees with Simon *et al.*,[7] Helleis *et al.*[8] and Kenner *et al.*[10] at $T = 298$ K. Simon *et al.*,[7] who report the greatest room temperature result of $k_1 = (3.1 \pm 1.9) \times 10^{-12}$ cm^3 molecule^{-1} s^{-1} is the only other work on reaction (1) to date that has used absorption spectroscopy to measure ClO (UV region) and HO$_2$ (IR region). Prior to the current work, the Simon *et al.*[7] investigation was the highest pressure study at $p = 240$ Torr, which when compared to the low pressure work of the other studies, led to the proposal that this relatively large reported value of k_1 may be indicative of a pressure dependence to reaction (1). However, recent studies have not observed a pressure dependence to k_1 between $p = 100 - 200$ Torr. When compared to the current work, which was carried out at around three times the pressure of Simon *et al.*,[7] there is also no discernible difference between this study and the other, low pressure work. Consequently it appears, from consensus, that stabilisation of any [CH$_3$OOOCl]* energised intermediate which may be formed in reaction (1) is inefficient at $T = 298$ K, with the important caveat that the current work has not made pressure dependent studies.

The discrepancies between the previous studies and those of Simon *et al.*[7] could potentially arise from the concentration profiles of ClO derived in their work, in which ClO absorption was measured at $\lambda = 292.2$ nm at the (6,0) band head of the ClO vibronic transition. Since the photolysis was continuous and modulated rather than pulsed, OClO was also inevitably formed which is a spectrally structured absorber whose spectrum overlaps that of ClO. Further, overlapping absorptions from HO$_2$, which absorbs more strongly over the same UV region as CH$_3$O$_2$, and other absorbers might also have introduced uncertainty into the [CH$_3$O$_2$]$_t$ profiles.

Such single wavelength studies may therefore be compared to the current work on which broadband UV spectroscopic measurements were made using differential spectroscopy to determine [ClO] unequivocally. While CH$_3$O$_2$ was unable to be directly monitored here, the

[ClO] measurements were unequivocal, utilising most of the ClO vibronic absorption spectrum. Further, the potential for secondary chemical effects on the observed rate constant is much higher in the Simon et al.[7] study than in this work owing to the non-selective and continuous photolysis of the gas mixtures in their study. As was evident in our work by the initial use of an overly simplistic chemical mechanism in the current work, secondary chemistry effects on the determined k_1 can certainly lead to an overestimation of this parameter if omitted from the analytical procedure.

The work reported here represents the first reported determination of the kinetics of reaction (1) as a function of temperature at atmospheric pressure using the flash photolysis technique using broadband UV absporption spectroscopic detection. The three previous temperature dependence studies of reaction all used the discharge-flow tube method. As shown in Figure 10, there is considerable disagreement in the parameterised temperature dependences (*i.e.* *E/R*) between these studies with only two agreeing on a positive temperature dependence (Helleis et al.[8] and Leather et al.[14]) albeit with different *E/R* values. The current work reports k_1 in best agreement with the most recently published work of Leather et al.[14] but also agrees with Helleis et al.[8] when considering the reported uncertainty and the 2 σ uncertainty (*i.e.* 95 %) of this work. There are a number of differences in the experimental setup of the Leather et al.[14] work and the two earlier studies of Helleis et al.[8] and Kukui et al.[11] which can perhaps explain the discrepancies between them, as summarised by Leather et al.[14]

Firstly, the two earlier studies[8,11] of reaction employed low pressures, $p = 2 - 5$ Torr, compared to $p = 100 - 200$ Torr in Leather et al.[14] and $p = 760$ Torr in the current work. These low pressure regimes were open to significant secondary chemistry effects owing principally to the incomplete (termolecular) conversion of the methyl radical, CH_3, into CH_3O_2 and therefore the possibility of side reactions of CH_3. For example, the CH_3 radical is known to react with ClO,[16] which might invoke a spurious loss of ClO, also producing CH_3O (thereafter HO_2) and also regenerating Cl (thereafter the original ClO and CH_3O_2 radicals):

$$ClO + CH_3 \rightarrow Cl + CH_3O \qquad (11)$$

Further, at the low pressures and therefore low $[O_2]$ used in the flow tube studies, the CH_3O formed could also react directly with ClO:

$$ClO + CH_3O \rightarrow HOCl + HCHO \qquad (12)$$

which has potential consequences of spurious product formation if unaccounted for.

Furthermore, both of the early studies employ the use of F atoms generated by a microwave discharge which react with CH_4 in an analogous fashion to reaction (6). However unlike in the present work, where effectively all the CH_3 generated reacts with O_2, there is up to a 40 % loss of F-to-CH_3O_2 conversion as reported by Kukui *et al.*,[11] implying there is significant unidentified secondary chemistry and radical loss taking place in these studies.

The different ion sources employed in the mass spectrometric detection might also help account for the discrepancies between the initial studies of reaction (1) and those of Leather *et al.*[14] Leather *et al.*[14] used time of flight chemical ionisation mass spectrometry (TOF CIMS) a far more selective and sensitive method of ionisation and detection compared to electron impact (EI) ionisation with quadrupole mass detection such as employed in the previous work. Further, CIMS is a softer ionisation technique compared to EI, which can often result in the fragmentation of parent ions into several fragments. This may be the case in the Helleis *et al.*[8] study which used Cl_2O to generate ClO. Cl_2O readily fragments to give Cl and ClO peaks upon EI mass detection, thereby potentially masking the actual ClO peak. Thus, in recognition of this and to mitigate this effect, Helleis *et al.*[8] used reduced $[Cl_2O]$, making it thereafter possible for excess Cl atoms to react with CH_3O_2 in the flow tube.

Wall losses of radicals also feature heavily in both the Helleis *et al.*[8] and Kukui *et al.*[11] work whereas the higher pressure regime of the Leather *et al.*[14] study operated under turbulent flow conditions which limited these effects. In the present work there are minimal heterogeneous effects to account for as the slow flowing atmospheric pressure photolysis mixture is probed along the central longitudinal axis of the reactor.

To conclude, the current work, whilst not making direct $[CH_3O_2]_t$ measurements, operated under conditions where these radical concentrations were well-constrained and in which secondary chemistry was minimised and accounted for in sensitivity studies. The results are not in accord with the original low pressure flow tube studies of reaction (1), but agree well with the more recent turbulent flow tube studies of Leather *et al.*[14] Such high pressure studies

enable the efficient formation of CH_3O_2 radicals and the minimisation of the production of HO_2 radicals leading to the preclusion of extensive secondary chemistry.

In comparison with previous work, the atmospheric implications of this work support those made by Leather *et al.*[14] The smaller rate constants reported in this work and in that of Leather *et al.*[14] imply that the importance of reaction (1) in both Spring Polar vortices is considerably less than previously estimated from the earlier temperature dependence studies. Leather *et al.*[14] estimate that the effectiveness of reaction (1) in converting CH_3O_2 to CH_3O is reduced by a factor of 1.5 contributing to only 10 % of this conversion. Furthermore, the effectiveness in the partitioning of active chlorine into the reservoir CH_3OCl species by reaction (1), which is believed to be the minor product channel of this reaction, becomes less significant due to the lower total rate constant k_1 at stratospheric temperatures (assuming the branching to channel (1c) is small). The strong positive temperature dependence reported here implies that the importance of reaction (1) in the troposphere is therefore be restricted to the low altitude and latitude regions such as the Southern Ocean where more ambient temperatures are typically found along with conditions of very low NO_x, BrO and IO (which all react more efficiently with ClO than CH_3O_2) and ClO levels are observed to be relatively high for the troposphere. However, under these conditions HO_2 levels also dominate over CH_3O_2 and HO_2 reacts with ClO more efficiently than CH_3O_2. Further, HO_2 radicals also react with CH_3O_2 itself. Thus the implications of the results presented here and in general agreement with the findings of Leather *et al.*[14] suggest overall a potentially modest effect of reaction (1) in the overall chemistry of the atmosphere, but one which has yet to be fully investigated through atmospheric modelling studies.

19

5. Conclusions

The kinetics of the ClO + CH$_3$O$_2$ reaction have been investigated as a function of temperature (T = 298 – 250 K) by the laser flash photolysis technique, using broadband UV absorption spectroscopy coupled to CCD detection at p = 760 Torr. This is the first study of this reaction using the flash photolysis technique as a function of temperature.

This work has found a significant positive activation energy for the ClO + CH$_3$O$_2$ reaction by measuring the decay of ClO through reaction with CH$_3$O$_2$ relative to the well defined kinetics of the reversible ClO self-reaction forming Cl$_2$O$_2$. Secondary chemistry has been found to potentially underestimate the positive temperature dependence of this reaction if unaccounted for. The results of this work are in agreement with those of Leather *et al.*[14] which operated over pressures of the same order of magnitude as in this work. The positive temperature dependence may limit the significance of the ClO + CH$_3$O$_2$ reaction under stratospheric conditions.

Table 1: Determinations (and NASA/ IUPAC recommendations) of the ambient and temperature dependence of k_1.

Study	T / K	k_1 /cm^{3}molec^{-1}s^{-1}	A / cm^{3}molec^{-1}s^{-1}	(E/R) /K
Simon et al.[7]	300	$(3.1 \pm 1.7) \times 10^{-12}$	-	-
Helleis et al.[8,9]	295	$(2.2 \pm 0.1) \times 10^{-12}$	3.25×10^{-12}	114 ± 38
Kenner et al.[10]	293	$(1.9 \pm 0.4) \times 10^{-12}$	-	-
Kukui et al.[11]	300	$(2.5 \pm 0.3) \times 10^{-12}$	2.0×10^{-12}	-80 ± 50
Leather et al.[14]	294	$(2.4 \pm 0.1) \times 10^{-12}$	$(2.0^{+0.28}_{-0.24}) \times 10^{-12}$	626 ± 35
JPL NASA[16]	298	$(2.2 \pm 0.92) \times 10^{-12}$	3.3×10^{-12}	115
IUPAC[17]	298	$(2.2 \pm 1.4) \times 10^{-12}$	2.40×10^{-12}	20
This work	298	$(2.7 \pm 0.5) \times 10^{-12}$	$(2.2^{+3.4}_{-1.30}) \times 10^{-12}$	642 ± 253

21

Table 2: Results from ClO dimerization kinetic studies and experimental determination of k_1.

T / K	$[ClO]_0{}^a$ / 10^{14}	k_8 / $10^{-13\,b}$	$k_{-8}{}^c$	$k_1{}^a$ / 10^{-12}
298.15	$1.00 - 1.30$	(5.63 ± 0.20)	36.06 ± 0.44	(2.73 ± 0.46)
287.05	(1.39 ± 0.06)	(6.96 ± 0.02)	14.46 ± 0.35	(2.30 ± 0.07)
276.85	(1.33 ± 0.23)	(7.53 ± 0.62)	4.84 ± 0.06	(2.48 ± 0.67)
270.1	(0.53 ± 0.02)	(11.18 ± 0.67)	1.24 ± 0.07	(1.52 ± 0.62)
267.25	(1.19 ± 0.05)	(9.15 ± 0.38)	1.49 ± 0.06	(2.57 ± 1.00)
263.1	(0.49 ± 0.07)	(11.73 ± 0.60)	0.03 ± 0.01	(1.24 ± 0.47)
258.3	(1.48 ± 0.11)	(9.83 ± 0.34)	0.40 ± 0.01	(2.06 ± 0.45)
249.95	(1.22 ± 0.04)	(10.00 ± 0.74)	0.10 ± 0.03	(2.14 ± 0.97)

^{a}*Units of molecules* cm^{-3}, ^{b}*units of* cm^3 *molecule*$^{-1}$ s^{-1}, ^{c}*units of* s^{-1}

Table 3: Full reaction scheme employed in modelling the ClO + CH$_3$O$_2$ kinetics. Rate constants were taken from the current NASA-JPL data evaluation.[16] *N.B.* Only salient reactions are numerically labelled.

	Reaction	Rate coefficient ($k(T)$ at 760 Torr)^{a}
	Principal Reaction	
(1a)	$ClO + CH_3O_2 \rightarrow ClOO + CH_3O$	$2.40 \times 10^{-12} \exp(-20/T)$
(1b)	$ClO + CH_3O_2 \rightarrow CH_3OCl + O_2$	$k_{af}/k_f = 1.51 \exp(-218/T)$
	Cl Chemistry	
(3)	$Cl + Cl_2O \rightarrow Cl_2 + ClO$	$6.20 \times 10^{-11} \exp(130/T)$
(8)	$ClO + ClO \rightarrow Cl_2O_2$	$k_0 = 1.60 \times 10^{-32} \times (T/300)^{-4.5b}$
(-8)	$Cl_2O_2 \rightarrow ClO + ClO$	$k_\infty = 3.00 \times 10^{-12} \times (T/300)^{-2}$
		$K_{eq} = 1.72 \times 10^{-27} \exp(8649/T)^{c}$
	$ClO + ClO \rightarrow Cl_2 + O_2$	$1.00 \times 10^{-12} \exp(1590/T)$
	$ClO + ClO \rightarrow OClO + Cl$	$3.50 \times 10^{-13} \exp(1370/T)$
	$ClO + ClO \rightarrow ClOO + Cl$	$3.00 \times 10^{-11} \exp(2450/T)$
	$Cl + O_2 \rightarrow ClOO$	$k_0 = 2.20 \times 10^{-33} \times (T/300)^{-3.1b}$
	$ClOO \rightarrow Cl + O_2$	$k_\infty = 1.80 \times 10^{-10} \times (T/300)^{0}$
		$K_{eq} = 6.60 \times 10^{-25} \exp(2502/T)^{c}$
	$ClO + HO_2 \rightarrow HOCl + O_2$	$2.60 \times 10^{-12} \exp(290/T)$
	$ClOO + ClOO \rightarrow ClO + ClO + O_2$	1.60×10^{-11}
	$ClOO + Cl_2 \rightarrow Cl_2O + ClO$	3.40×10^{-12}
	$ClO + OClO \rightarrow Cl_2O_3$	$k_0 = 5.80 \times 10^{-33} \times (T/300)^{-4.7b}$
	$Cl_2O_3 \rightarrow ClO + OClO$	$k_\infty = 2.40 \times 10^{-11} \times (T/300)^{-1.1}$
		$K_{eq} = 1.50 \times 10^{-27} \exp(7140/T)^{c}$
	$Cl + Cl_2O_2 \rightarrow Cl + Cl_2 + O_2$	1.00×10^{-10}
	CH$_3$O Chemistry	
	$CH_3O + CH_3O \rightarrow HCHO + CH_3OH$	3.80×10^{-11}
	$CH_3O_2 + CH_3O \rightarrow HCHO + CH_3OOH$	5.00×10^{-13}
	$CH_3O + ClO \rightarrow HOCl + HCHO$	3.40×10^{-11}
	$CH_3O + HO_2 \rightarrow HCHO + H_2O_2$	5.00×10^{-13}
(10)	$CH_3O + O_2 \rightarrow HO_2 + HCHO$	$3.90 \times 10^{-14} \exp(-900/T)$
	$CH_3O + CH_4 \rightarrow CH_3OH + CH_3$	$2.61 \times 10^{-13} \exp(-4450/T)$
	CH$_3$O$_2$ Chemistry	
	$Cl + CH_4 \rightarrow HCl + CH_3$	$7.30 \times 10^{-12} \exp(-1280/T)$
	$CH_3 + O_2 \rightarrow CH_3O_2$	$k_0 = 4.00 \times 10^{-31} \times (T/300)^{-3.6b}$
		$k_\infty = 1.20 \times 10^{-12} \times (T/300)^{1.1}$

(9a)	$CH_3O_2 + CH_3O_2 \rightarrow CH_3O + CH_3O + O_2$	$9.50 \times 10^{-14} \exp(390/T)k_{9a} / k_9$, with
(9b)	$CH_3O_2 + CH_3O_2 \rightarrow HCHO + CH_3OH + O_2$	$k_9 = (26.2 \exp(-1130/T) + 1)$
	$HO_2 + CH_3O_2 \rightarrow CH_3OOH + O_2$	$4.10 \times 10^{-13} \exp(750/T)$
	$Cl + CH_3O_2 \rightarrow ClO + CH_3O$	3.845×10^{-11}
	$Cl + CH_3O_2 \rightarrow HCl + CH_2O_2$	3.85×10^{-11}

HO₂ Chemistry

$HO_2 + HO_2 \rightarrow H_2O_2 + O_2$	$3.00 \times 10^{-13} \exp(460/T) + 5.17 \times 10^{-14} \exp(920/T)$
$HO_2 + CH_3OH \rightarrow HO_2.CH_3OH$	$2.80 \times 10^{-15} \exp(-1800/T)$
$HO_2.CH_3OH \rightarrow HO_2 + CH_3OH$	$K_{eq} = 1.10 \times 10^{-24} \exp(4093/T)^c$
$HO_2 + HO_2.CH_3OH \rightarrow H_2O_2 + CH_3OH + O_2$	$5.40 \times 10^{-11} \exp(-410/T)$
$HO_2 + H_2O \rightarrow HO_2.H_2O$	$2.80 \times 10^{-15} \exp(-180/T)$
$HO_2.H_2O \rightarrow HO_2 + H_2O$	$K_{eq} = 2.40 \times 10^{-25} \exp(4350/T)^c$
$HO_2 + HO_2.H_2O \rightarrow H_2O_2 + H_2O + O_2$	$5.40 \times 10^{-11} \exp(-410/T)$
$HO_2 + Cl \rightarrow HCl + O_2$	$1.40 \times 10^{-1} \exp(270/T)$
$HO_2 + Cl \rightarrow OH + ClO$	$3.60 \times 10^{-11} \exp(-375/T)$
$Cl + H_2O_2 \rightarrow HCl + HO_2$	$1.10 \times 10^{-11} \exp(-980/T)$
$Cl + CH_3OH \rightarrow CH_2OH + HCl$	5.50×10^{-11}
$CH_2OH + O_2 \rightarrow HCHO + HO_2$	9.10×10^{-11}

Secondary Chemistry

$Cl + CH_3Cl \rightarrow CH_2Cl + HCl$	$2.17 \times 10^{-11} \exp(-1130/T)$
$CH_2Cl + O_2 \rightarrow CH_2ClO_2$	$k_0 = 1.90 \times 10^{-30} \times (T/300)^{-3.2b}$
	$k_\infty = 2.90 \times 10^{-12} \times (T/300)^{1.1}$
$CH_2ClO_2 + HO_2 \rightarrow CH_2ClOOH + O_2$	$3.30 \times 10^{-13} \exp(820/T)$
$CH_3 + Cl_2 \rightarrow CH_3Cl + Cl$	$1.61 \times 10^{-12} \exp(64/T)$
$CH_3 + Cl \rightarrow CH_3Cl$	6.11×10^{-11}
$HO_2 + HCHO \rightarrow HOCH_2O_2$	$9.70 \times 10^{-15} \exp(-625/T)$
$HOCH_2O_2 \rightarrow HO_2 + HCHO$	$2.40 \times 10^{12} \exp(7000/T)$
$HOCH_2O_2 + HO_2 \rightarrow HOCH_2OOH + O_2$	$5.60 \times 10^{-15} \exp(-2300/T)$
$HOCH_2O_2 + HO_2 \rightarrow O_2 + HC(O)OH + H_2O$	$0.65.60 \times 10^{-15} \exp(-2300/T)$
$HOCH_2OOH + Cl \rightarrow HCOOH + OH + HCl$	1.00×10^{-10}
$HOCH_2OOH + Cl \rightarrow HOCH_2O_2 + HCl$	5.00×10^{-10}
$HOCH_2O_2 + HOCH_2O_2 \rightarrow 2HOCH_2O + O_2$	$5.70 \times 10^{-14} \exp(750/T)$
$HOCH_2O_2 + HOCH_2O_2 \rightarrow HCOOH + CH_2O_2H_2 + O_2$	5.50×10^{-12}
$HOCH_2O_2 + O_2 \rightarrow HCOOH + HO_2$	3.50×10^{-14}

$CH_3 + CH_3 \rightarrow C_2H_6$	2.41×10^{-13}
$CH_3OOH + Cl \rightarrow HCl + CH_2OOH$	$8.10 \times 10^{-11} \exp(30/T)$
$Cl + HCHO \rightarrow HCl + HCO$	$3.50 \times 10^{-12} \exp(140/T)$
$HCO + O_2 \rightarrow CO + HO_2$	$6.10 \times 10^{-12} \exp(-36/T)$

[a]Units are cm^3 molecule^{-1} s^{-1} unless otherwise stated [b]units of cm^6 molecule^{-2} s^{-1} and [c]units of cm^3 molecule^{-1}

Figure Captions

Figure 1: Absorption cross sections of the key absorbing species present in the photolysed Cl_2/ Cl_2O/ CH_4/ O_2 system. ClO (black); CH_3O_2 (blue); HO_2 (pink); Cl_2O_2 (light green); Cl_2O (red); $Cl_2 \times 10$ (light blue); HOCl $\times 10$ (green); $CH_3OCl \times 10$ (orange).

Figure 2: Typical time averaged absorption spectra from photolysis (relative to pre-photolysis) of Cl_2/ Cl_2O/O_2/N_2 mixtures recorded in the absence of methane (black) and in the presence of $(6.0 \times 10^{15}$ molec cm$^{-3})$ methane (red).

Figure 3: ClO temporal traces recorded from a series of sequential photolysis experiments (laser photolysis at t = 0.028 s), at T = 287 K as a function of $[CH_4]$/ molec cm^{-3}: $[CH_4] = 0$ (black); $[CH_4] = 3.10 \times 10^{18}$ (blue); $[CH_4] = 5.25 \times 10^{18}$ (red); $[CH_4] = 7.40 \times 10^{18}$ (green); and $[CH_4]$ *restored to 0* (yellow).

Figure 4: Initial post photolysis [ClO] recorded as a function of added methane, at T = 298 K. The solid line shows a fit to initial [ClO] using JPL NASA kinetic parameters, with an initial concentration of $[Cl_2O] = 7.40 \times 10^{18}$ molec cm^{-3}.

Figure 5: van't Hoff plot of the equilibrium constant K_8 (black squares) compared to values reported by Ferracci *et al.*[19] (red squares)

Figure 6: [ClO] temporal trace with a simulation incorporating ClO dimerization only kinetics from observed $[ClO]_0$.

Figure 7: Diagrammatic representation of reaction pathways in the ClO + CH_3O_2 reaction.

Figure 8: Typical [ClO] temporal trace from the ClO + CH_3O_2 reaction and fit from numerical integration.

Figure 9: Arrhenius plot for k_1 taken from the current investigation.

Figure 10: Arrhenius plot comparing the experimental data of this work (red squares and line) and the parameterisations of the work reported by: Helleis *et al.*[8] (black); Kukui *et al.*[11] (blue); Leather *et al.*[14] (green).
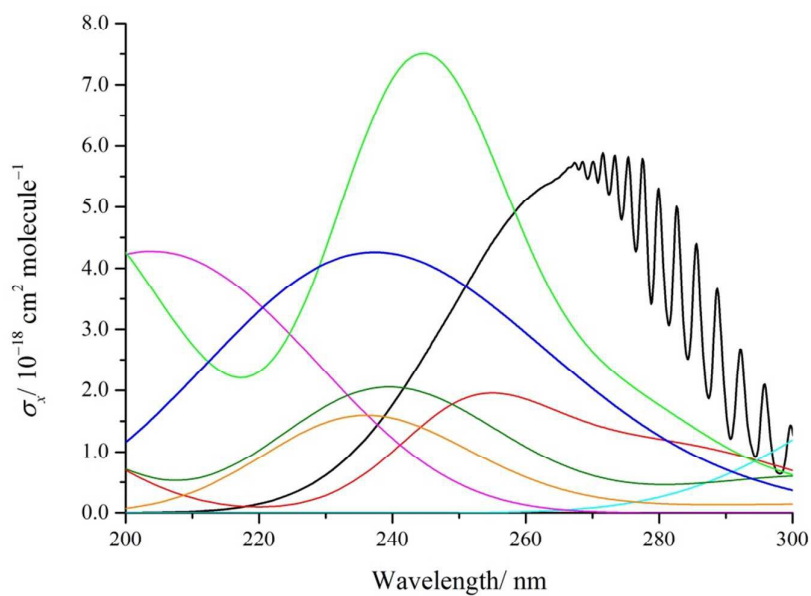
Figure 1:
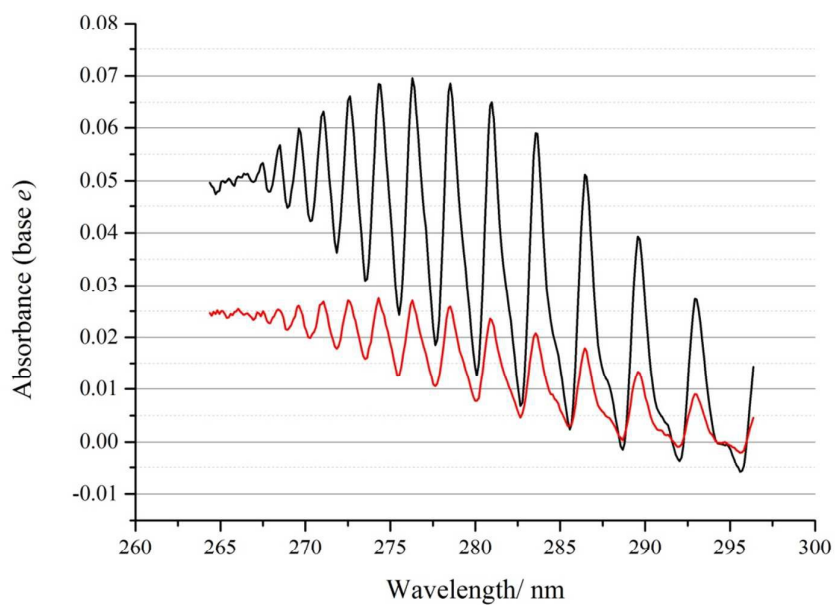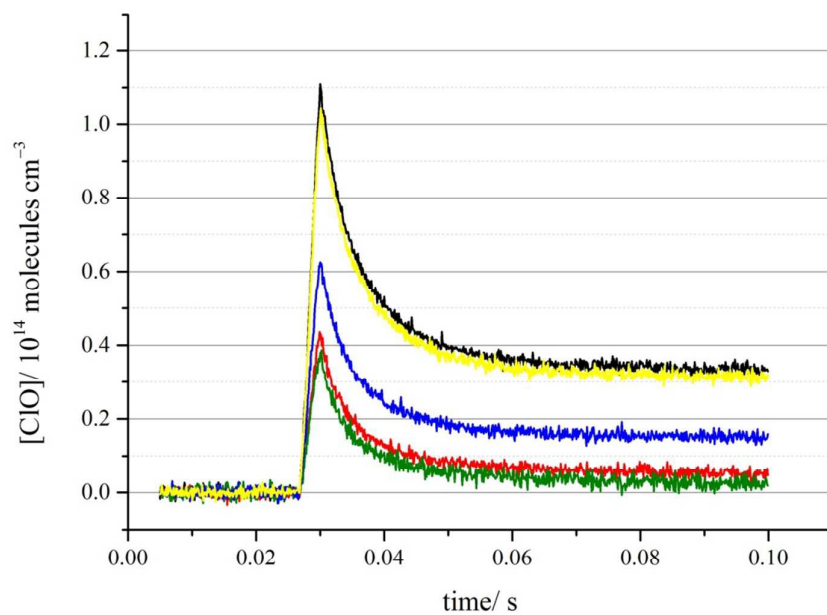
Figure 2:

Figure 3:

Figure 4:
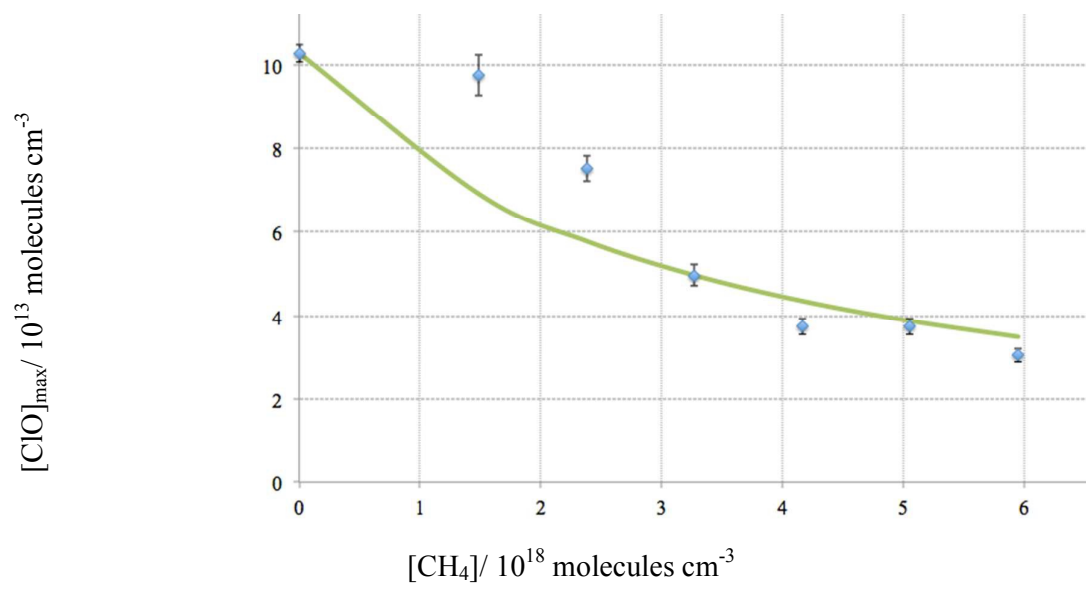
Figure 5:
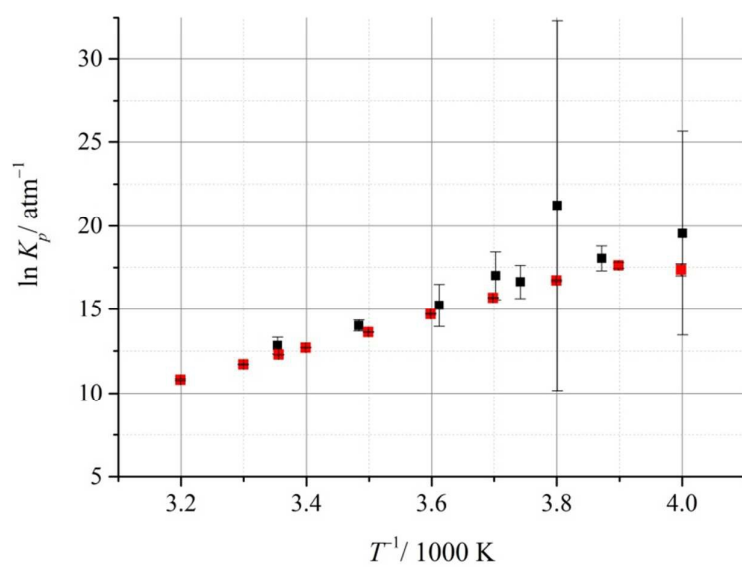
Figure 6:
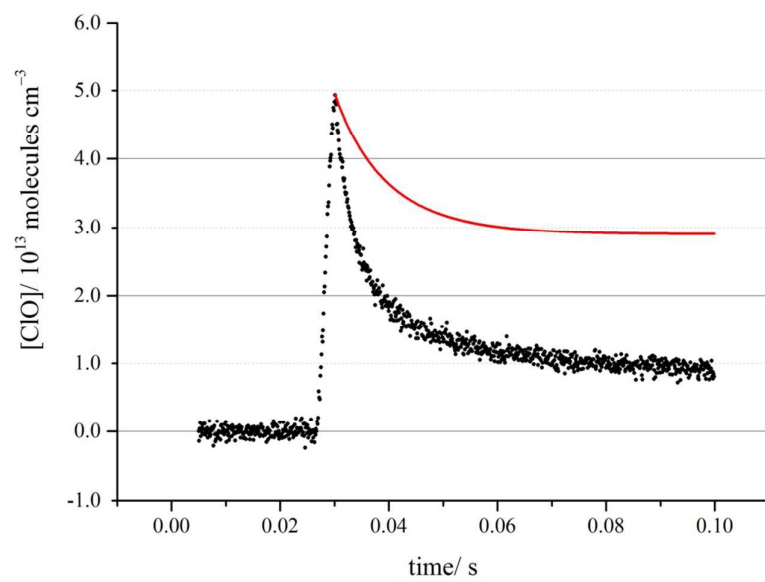
Figure 7:
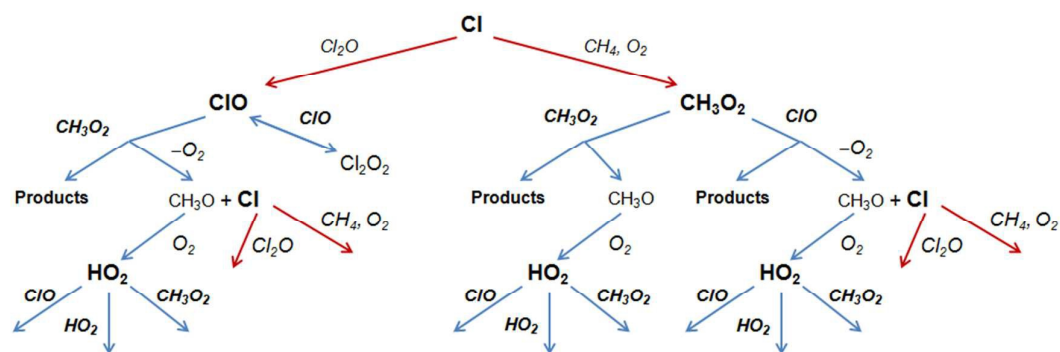
Figure 8:

Figure 9:

Figure 10:

Physical Chemistry Chemical Physics Accepted Manuscript

Physical Chemistry Chemical Physics Accepted Manuscript

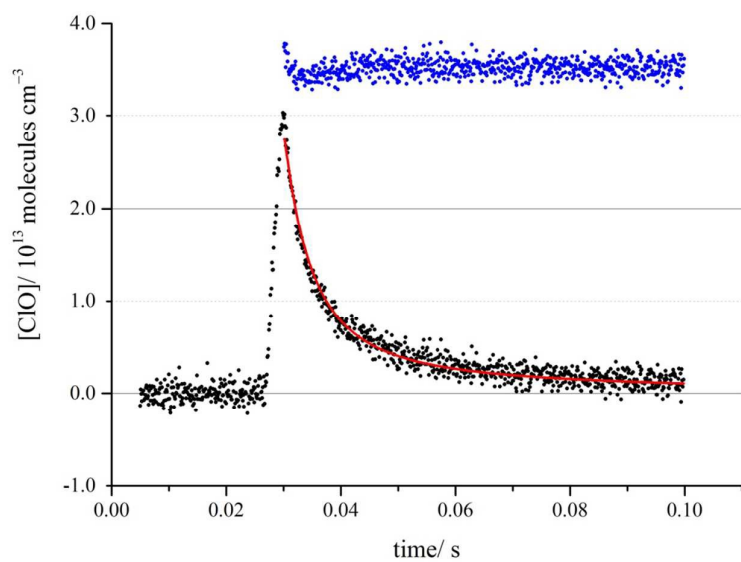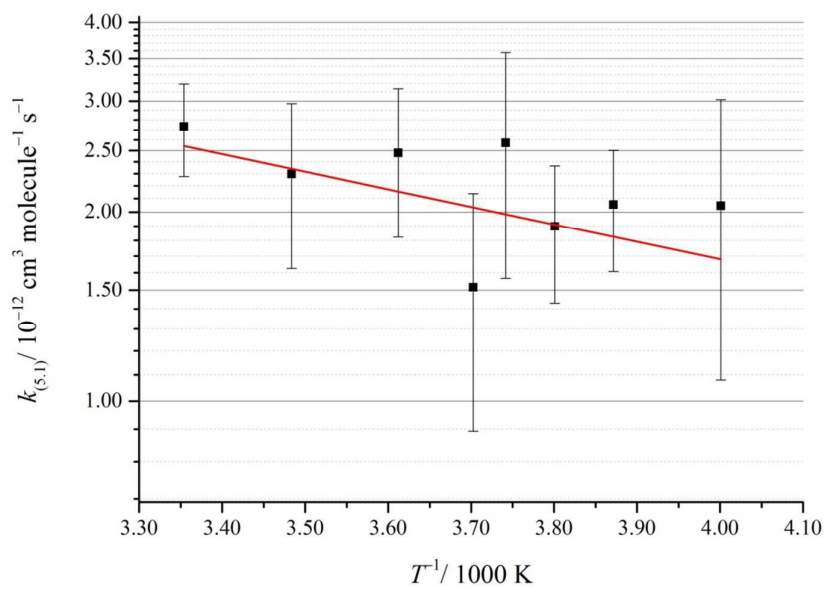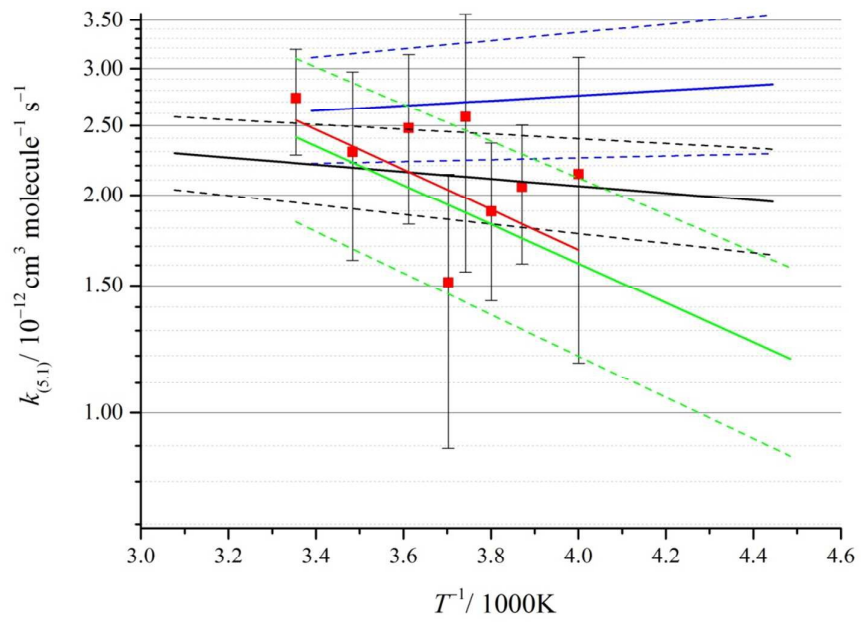**References**

1 Saiz-Lopez, M, *et al. Atmos Chem. Phys.*, 2012, **12**. P 3939. DOI: 10.5194/acp-12-3939-2012.

2 Molina, L.T. and M.J. Molina,. *J. Phys. Chem.* 1987. **91**(2): 433-436.

3 Lee, A.M., R.L. Jones, I. Kilbane-Dawe, I, J.A. Pyle., *J. Geophys Res. Atmospheres*, 2002, **107**, D11, DOI 10.1029/2001JD000538.

4 Hossaini, R, M.P. Chipperfield, S.A. Montzka, A. Rap, S. Dhomse, W. Feng, *Nature Geoscience,* 2015, **8** (3), 186.

5 M.K.M. Ward and D.M. Rowley, *Physical Chemistry Chemical Physics*, 2016, DOI: 10.1039/C5CP07329D

6 Crutzen, P.J, R. Muller, C. Bruhl and Th. Peter, *Geophys Res Let*, 1992. **19** (11): 1113.

7 Simon, F.G., J.P. Burrows, W. Schneider, G.K. Moortgat and P.J. Crutzen, *J. Phys. Chem.,* 1989. **93** (23): 7807.

8 Helleis, F, J.N. Crowley and G.K.Moortgat, *J. Phys. Chem*, 1993. **97** (44): 11464.

9 Helleis, F, J.N Crowley and G.K. Moortgat, *Geophys. Res. Let.* , 1994. **21** (17): 1795.

10 Kenner, R.D., K.R. Ryan, and I.C. Plumb,. *Geophys. Res. Let.*, 1993. **20** (15): 1571.

11 Kukui, A.S., T.P.W. Jungkamp, and R.N. Schindler,. *Berichte Der Bunsen-Gesellschaft-Physical Chemistry Chemical Physics*, 1994. **98**(10): 1298.

12 Biggs, P., C.E. Canosa-mas, J.M. Fracheboud, D.E. Shallcross, and R.P. Wayne, *Geophys. Res. Let.*, 1995. **22** (10): 1221.

13 Daele, V. and G. Poulet, *Journal De Chimie Physique et De Physico-Chimie Biologique*, 1996. **93** (6): 1081.

14 Leather, K.E., A. Bacak, R. Wamsley, A.T. Archibald, A. Husk, D.E. Shallcross, and C.J. Percival, *Physical Chemistry Chemical Physics*, 2012. **14** (10): 3425.

15 R. Muller *et al.* Geophys. Res. Lett., 1994, 21, 1427–1430

[16] Sander, S.P., J. Abbatt, J. R. Barker, J. B. Burkholder, R. R. Friedl, D. M. Golden, R. E. Huie, C. E. Kolb, M. J. Kurylo, G. and V.L.O. K. Moortgat, P. H. Wine, *"Chemical Kinetics and Photochemical Data for Use in Atmospheric Studies, Evaluation No. 17"* JPL Publication 10-6, Jet Propulsion Laboratory, Pasadena, 2011 http://jpldataeval.jpl.nasa.gov

[17] Kosmas, A.M. and E. Drougas, *Chemical Physics*, 2009. **358**(3): 230-234.

[18] Hinshelwood, C.N. and C.R. Prichard*., Journal of the Chemical Society*, 1923. **123**: 2730.

[19] Ferracci, V, *PhD thesis*, University of London, 2012.

[20] Ward, M.K.M, *PhD thesis*, University of London, 2015.

[21] Ferracci, V. and D.M. Rowley*, Physical Chemistry Chemical Physics*, 2014. **16** (3): 1182.

[22] Ferracci, V. and D.M. Rowley*, Physical Chemistry Chemical Physics*, 2010. **12**(37): 11596.

[23] Ferracci, V. and D.M. Rowley, Int J. Chem. Kinetics, 2012, 44 (6), 386.

[24] Boakes, G., W.H.H. Mok, and D.M. Rowley, *Physical Chemistry Chemical Physics*, 2005. **7** (24): 4102-4113.